Computers and Concrete, *Vol. 26, No. 2 (2020) 161-173*
DOI: https://doi.org/10.12989/cac.2020.26.2.161

Shear strength of match-cast-free dry joint in precast girders

Haibo Jiang[a], Jiahui Feng, Jie Xiao*, Mingzhu Chen and Weibin Liang

School of Civil and Transportation Engineering, Guangdong University of Technology, Guangzhou Higher Education Mega Center, Guangzhou 510006, China

(*Received March 1, 2019, Revised July 8, 2020, Accepted July 28, 2020*)

Abstract. Shear keys in precast concrete segmental bridges (PCSBs) are usually match-casting which is very labour intensive. In this research, an innovative match-casting-free construction was proposed by leaving small gap between the convex and the concave castellated shear keys in the joints of PCSBs. Specimen experiment, shear strength analysis and numerical simulation were conducted, investigating the loading performance of this new type of dry joints, the gap dry joints. Compared with match-casting joint specimens, it has been found from experiment that shear capacity of gap joint specimens significantly decreased ranging from 17.75% to 42.43% due to only partially constrained and contacted in case of gap dry joints. Through numerical simulation, the effects of bottom contacting location, the heights of the gap and the shear key base were analyzed to investigate strength reduction and methods to enhance shear capacity of gap joint specimens. Numerical results proved that shear capacity of gap dry joints under full contact condition was higher than that under partial contact. In addition, left contact destroyed the integrity of shear keys, resulting in significant strength reduction. Larger shear key base remarkably increased shear capacity of the gap joint. Experimental tests indicated that AASHTO provision underestimated shear capacity of the match-casting dry joint specimens, while the numerical results for the gap dry joint showed that AASHTO provision underestimated shear capacity of full contact specimens, but overestimated that of left contact specimens.

Keywords: direct shear; matching joint; gap joint; strength reduction; code evaluation; numerical simulation

1. Introduction

The superstructures of precast concrete segmental bridges (PCSBs) are widely constructed by means of assembling the precast box girder segments with subsequent prestressing. Factory orientation, mechanization and standardization are required in modern bridge construction, aiming to achieve high construction speed and control precision (Wang *et al*. 2014). The short-line match-casting method is the most common construction technology in externally or internally prestressed PCSBs.

Standardized construction process of short-line match-casting method is shown in Fig. 1(a). After the newly cast beam segment (concrete segment 2) curing for 7 days, the mold beam segment (concrete segment 1) is moved away and stored, and then the concrete segment 2 is moved to the mold position and used as partial mold for the production of the new pouring beam segment (concrete segment 3). Standardized construction process repeats the step of erecting adjustment bottom formwork and side keyed plate, placing reinforcement cage, pouring concrete and curing. In this way, the beam segments are produced matchingly against one another in a factory to create tight matching surfaces when placed into the bridges.

Nevertheless, the negative aspects of match-casting construction are also evident. The end of the concrete segment 2 is required as the side template for the concrete segment 3. Before pouring the concrete segment 3, the concrete segment 2 requires 7 days for curing. Besides, the concrete segment 2 has to be moved to the mold position, then the bottom formwork and side keyed plate are adjusted. It leads to a relatively long construction period, multiple movements of beam segments and repeatedly erecting adjustment.

To overcome the disadvantages of the match-casting construction, an innovative dry joint in PCSBs is proposed as the first time in this research for the match-casting-free construction. As illustrated in Fig. 1(b), match-casting-free construction highlights that girder components are precast independently by providing a gap joint between the male and female part of dry joint, which can overcome the allowable alignment error. The convex shear key is smaller than the castellated concave surface on the adjacent segments, thereby giving a much easier way to assemble with the gap.

Obviously, the positive features of the match-casting-free construction include that it does not require the repeatedly erecting adjustment on the bottom formwork and repeatedly movement of the concrete segments. The mold position and pouring position are combined, thus the adjacent segments are produced independently and simultaneously. A gap joint for match-casting-free method costs shorter construction period and lower energy, and less labour intensive compared with short line alignment match-cast construction method.

However, match-casting-free construction may reduce

*Corresponding author, Assistant Professor
E-mail: xiaojie2017@gdut.edu.cn
[a]Professor
E-mail: hbjiang@gdut.edu.cn

http://www.techno-press.org/?journal=cac&subpage=8 ISSN: 1598-8198 (Print), 1598-818X (Online)

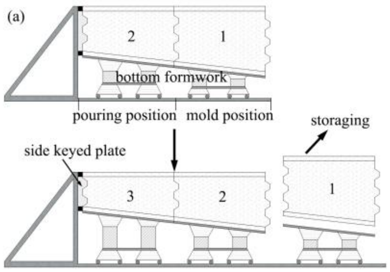

(a) Match-casting

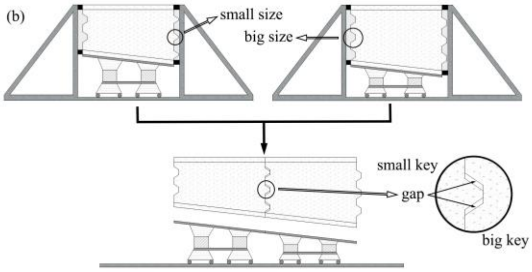

(b) Match-casting-free

Fig. 1 Construction methods for precast segments

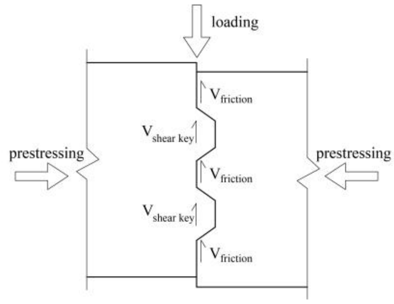

(a) Shear mechanisms of joints

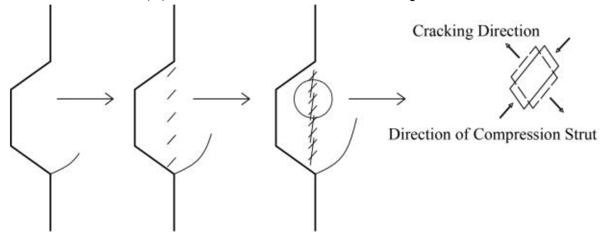

(b) Crack sequence

Fig. 2 Shear mechanisms and crack sequence for matching keyed dry joint

shear capacity of PCSBs. Enhancing shear capacity of the gap joint is possible, such as changing the dimensions and configurations of shear keys (Alcalde *et al*. 2013, Williams *et al*. 2017, Jiang *et al*. 2019), using high performance concrete (Lee *et al*. 2011, Kim *et al*. 2015, Liu *et al*. 2019), and applying higher confining stress (Jiang *et al*. 2015, Shamass *et al*. 2015, Bu and Wu 2018).

Higher concrete strength in dry joints can effectively enhance the cracking load and ultimate load (Jiang *et al*. 2016a). Normal concrete leads to a brittle failure of shear keys, but shear resistance of dry joints with steel fiber-reinforced concrete is improved because of its high rupture strength (Jiang *et al*. 2016b). Nowadays, using ultra-high performance concrete (UHPC) can reduce shear keys' cracking load and enhance load transfer for its superior strength and durability (Hussein *et al*. 2017). Direct shear tests of UHPC joints show that a higher shear strength of UHPC joints can be achieved, due to higher matrix tensile strength and the addition of steel fibers (Liu *et al*. 2019). Compared with ordinary concrete, the UHPC joints achieves much enhanced ductile behavior (Jang *et al*. 2017).

Shear mechanisms of keyed dry joints, as shown in Fig. 2(a), are the work of the support capacity of the shear key and friction resistance due to external compression forces perpendicular to the interface (AASHTO 2003, Turmo *et al*. 2006). Therefore, applying higher confining stress could increase shear capacity of the joints (Turmo *et al*. 2012, Shamass *et al*. 2015). The support effect of shear keys is reflected in the crack sequence, as depicted in Fig. 2(b). A number of diagonal compression struts are formed in the shear key base corresponding to multiple diagonal cracks, including only compressive stresses and tensile stresses, in the direction of the compression struts and in the cracking direction transverse to the compression struts, respectively (Kaneko *et al*. 1993).

Previous tests, however, are not directly applicable to shear transfer encountered in a gap joint. To the best of the authors' knowledge, very few tests are available to study specific shear transfer mechanism and simulate the surface details of the gap joint specimen. The present research involves the experimental test and the numerical simulation for match-casting and gap dry joint specimens.

This paper emphasizes on shear failure mechanism, shear strength reduction and Code evaluation of shear key in the gap joint by direct shear testing. In numerical simulation, the parameters investigated include the effect of bottom contacting location, the gap height and the height of shear key base, in order to find out strength reduction and methods to enhance shear capacity of gap joint specimens. The experimental and numerical shear capacities were also compared with those predicted by AASHTO provision in this research.

2. Experimental program

2.1 Specimens design and nomenclature

Matching joint specimen: A specimen was constructed by a short-line match-casting method with no gap in shear key, creating tight matching surfaces.

Gap joint specimen: A specimen was constructed by an independently casting method, with a gap locating at the top and bottom, respectively, of a shear key for match-casting-free construction.

The matching joint specimen and the gap joint specimen were illustrated in Fig. 3, consisting of two L-shaped components (i.e., the female and male parts). For the case of matching joint specimens, the female part was fabricated first. Then the male part was cast with the female part as a mold. The configuration and the fabricated procedure of matching joint specimens are similar to those adopted by Jiang *et al*. (2015, 2019). For the case of gap joint specimens, a 5-mm-height gap are designed at the top and

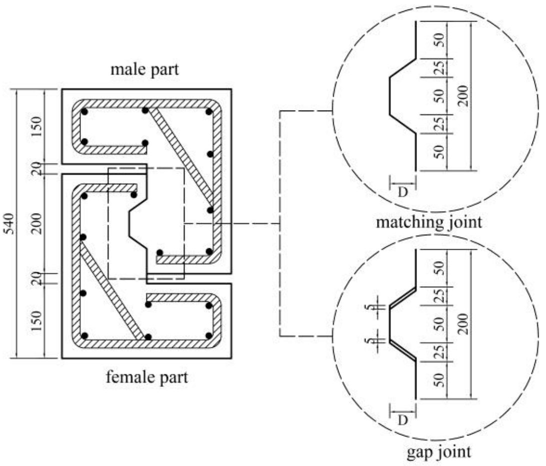

Fig. 3 Dimensions of specimens (unit: mm)

Table 1 Parameter of specimens

Specimens	Construction method	Joint type	Key depth (mm)	Confining stress (MPa)
S1-D2-#	match-casting	Matching joint	35	0.5/1.0/2.0
S2-D1-#	match-casting-free	Gap joint	25	0.5/1.0/2.0
S2-D2-#	match-casting-free	Gap joint	35	0.5/1.0/2.0
S2-D3-#	match-casting-free	Gap joint	45	0.5/1.0/2.0

Note: “#” in specimen notations represents for confining stress, corresponding to 0.5, 1.0 and 2.0 MPa.

bottom, respectively, of a shear key assembly. To prepare the gap joint specimens, two steel plates with a thickness of 5 mm are applied to the shear key mold prior to placing concrete. Therefore, the shear key in the male part is smaller than the concave surface in the female part. It should be noted that the female and male parts in the gap joint specimens can be fabricated simultaneously.

In total, twelve push-off specimens are tested under direct shear in this research. As listed in Table 1, all specimens are identified using the convention: (S1, S2) - (D1, D2 and D3) - (0.5, 1.0 and 2.0). This research is composed of two series of push-off test of dry keyed joints, i.e., matching joint specimens and gap joint specimens (corresponding to S1 and S2, respectively). In addition, shear key depth provided at the interface includes 25 mm, 35 mm and 45 mm (corresponding to D1 to D3, respectively). Initial prestressing level of confining stress acts on the joint surface before the vertical load applies, including 0.5, 1.0 and 2.0 MPa. As an example, S1-D2-0.5 denotes a matching joint specimen with 35-mm depth shear key under 0.5 MPa confining stress initially.

2.2 Material properties

The concrete used for casting all specimens is expected to get a compressive strength of 65 MPa after curing for 28 days. Concrete properties were tested, including compressive strength, splitting tensile strength, modulus of elasticity, and Passion’s ratio. All properties were measured on Φ150 mm×300 mm standard cylinders according to ASTM Codes. The results are shown in Table 2.

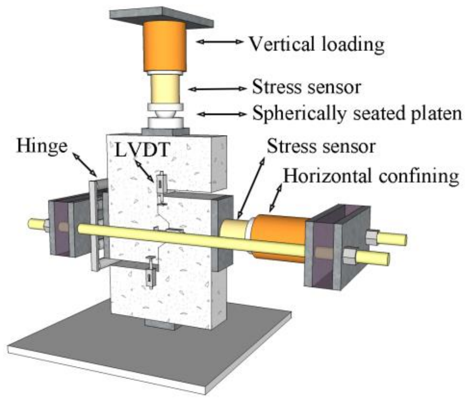

Fig. 4 Schematic of test setup and instrumentation

Table 2 Mechanical properties of concrete

Mechanical properties	Values	
	Matching joint	Gap joint
Target compressive strength (MPa)	65	65
Compressive strength f'_c (MPa)	68.88	64.21
Splitting tensile strength f_t (MPa)	4.77	4.37
Modulus of elasticity E_c (MPa)	34840	35020
Passion’s ratio μ	0.204	0.204

2.3 Test setup and procedure

A typical push-off test setup is adopted to study shear behavior of PCSBs as illustrated in Fig. 4. Detailed descriptions of the test setup can be obtained in Jiang *et al*. (2015 and 2019). All tests were carried out using a displacement-controlled scheme, with a loading step of 0.05 mm/minute. The deformations of the specimens are monitored, including the vertical displacement and the horizontal dilation between the male and female parts. Moreover, data obtained during test include the vertically applied loads and the horizontal confining forces acquired by relevant load cells.

3. Experimental results of matching joint specimens

3.1 Failure behavior and shear mechanism

Fig. 5 depicted the cracking patterns of shear key observed in matching joint specimens. The typical mode of failure observed from matching joint specimens involving a single curvilinear crack near the bottom corner of the shear key and multiple diagonal cracks along with shear key base plane. Due to high shear stress concentration, the single curvilinear crack was generated, but it tended to stop propagating for releasing little strain energy when it ran into a low-stress zone. Further applying load on, the multiple diagonal cracks along the key base were generated, forming a shear zone. A number of diagonal compression struts were formed along with the shear key base plane. Because of the highly localized strain distribution, eventually, multiple diagonal cracks were coalesced, leading to the final shearing off failure of the key.

The overall shear resistance was mainly depended on

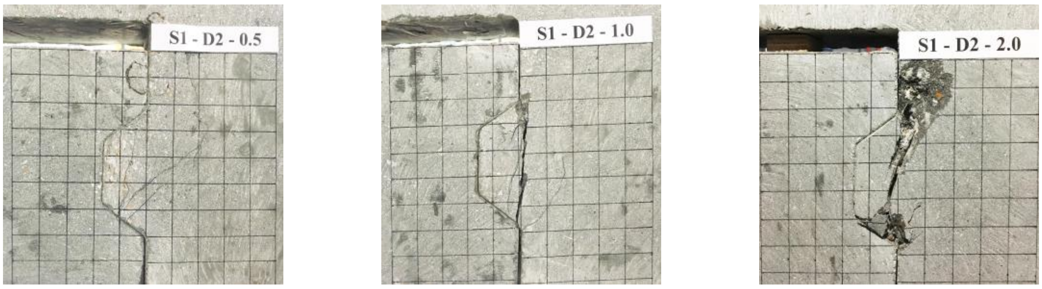

(a) (b) (c)

Fig. 5 Failure crack patterns of matching joint specimens

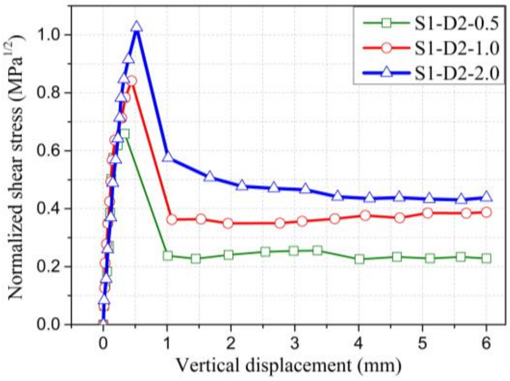

Fig. 6 Normalized shear stress–vertical displacement relations for matching joint specimens

the support capacity of shear key and the friction resistance. When the tensile stress exceeds tensile strength of concrete, the crack broke the integrity of a shear key, reducing the support capacity of the shear key. Eventually, the support capacity of the shear key eliminated on account of the failure of the shear key, thus the residual load-bearing behavior was dominated by friction resistance.

3.2 Normalized shear stress–vertical displacement curves

The normalized shear stress–vertical displacement responses of the matching joint specimen tests were illustrated in Fig. 6. Normalized shear stress is defined as the applied load divided by the area of the whole joint and $\sqrt{f_c'}$.

The total effect of the support capacity of a shear key and friction force provided shear resistance, showing a vertically ascending curve. The stiffness was a constant before the crack occurred, whereas the stiffness reduced due to the propagating of the cracks. The curve showed a significant reduction of shear strength after the applied load overcame the peak resistance, which was caused by the failure along the shear key base plane. After that, residual resistance remained a horizontal plateau, which was sustained mainly through aggregate interlock between the cracked shear key base plane and the friction along the smooth surface.

4. Experimental results of gap joint specimens

4.1 Failure behavior and shear mechanism

The failure crack patterns observed from the gap joint specimens are summarized in Fig. 7. Cracking mechanisms as illustrated in Fig. 8 involves a single inclined crack (*S* crack) and multiple diagonal cracks.

S crack appeared at right bottom corner (defined as S_R crack) or at left bottom corner (defined as S_L crack), as shown in Fig. 8. These phenomena were caused by the different contacting locations of the key bottom in the interface: (1) The key bottom might parallel to the concave bottom (full contact). (2) The key bottom might contact the concave bottom at the right corner first (right contact). (3) The key bottom might contact the concave bottom at the left corner first (left contact).

4.1.1 Full contact or right contact

The key bottom either parallel to the concave bottom or contacted at the right bottom corner first, and the two cases would generate a compression strut at the shear zone. Similar to shear failure of matching specimens, S_R crack occurred at right corner on shear key.

After that, multiple diagonal cracks occurred along with the key base plane, where a great many diagonal compression struts were formed. Eventually, the key was totally sheared off. Failure along the shear key base was direct shear failure, as illustrated in Figs. 7 (b, d, f and g).

4.1.2 Left contact

For the case of contacting the concave bottom at the left corner first**,** however, the first crack S_L initiated at the left bottom of male key and ended at the top of key base. The left top part of the key was sheared off first, and shear stress would be redistributing on the remainder of the key.

Further loaded to failure, multiple diagonal cracks were generated, but aslant crossing the shear key base plane. Failure crossing shear key base was diagonal shear, as illustrated in Figs. 7 (a, c, e, h and i).

4.2 Normalized shear stress–vertical displacement curves

The normalized shear stress–vertical displacement responses of the gap joint specimens were depicted in Fig. 9. Five stages can be divided from the initial loading to the terminal of test.

The first stage: When load was applied, shear strength

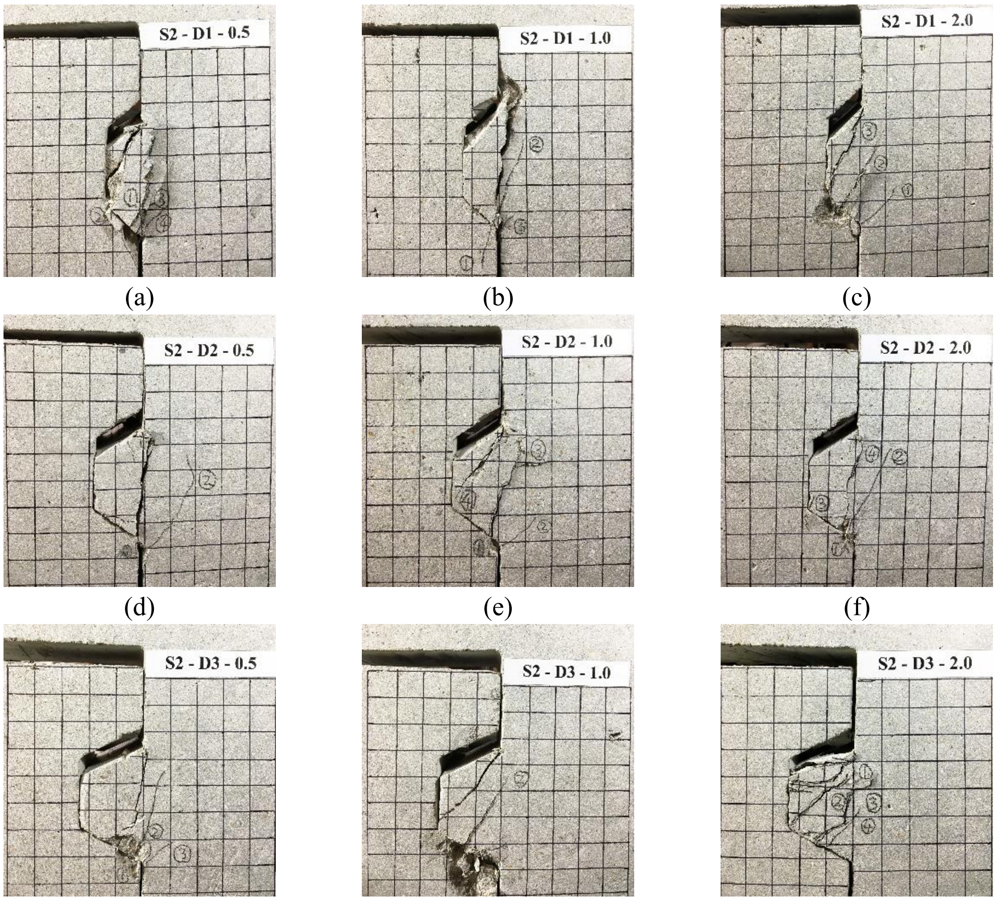

(a) (b) (c)

(d) (e) (f)

(g) (h) (i)

Fig. 7 Failure crack patterns of gap joint specimens

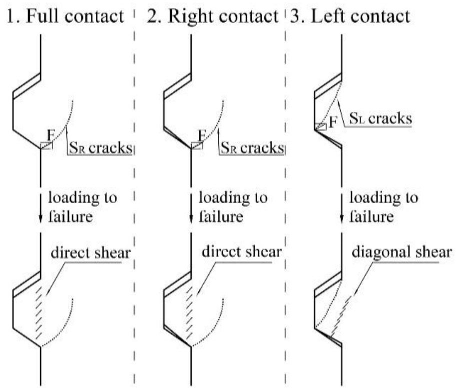

Fig. 8 Force analysis of crack propagation in gap joint

immediately rose to a certain level. It can be observed that there was just a small slip between the surfaces (see Fig. 9), the panel resisted the displacement by the friction coefficient.

The second stage (Initial resistance stage): The curve of shear resistance maintained a long horizontal plateau (see Fig. 9) until the contact of the key bottom took place, which was dominated by the friction due to a confining stress acted on the horizontal direction. Friction in the shear interface was produced because the rough surface with small protuberances resisted against the vertical displacement. A polishing effect made the small

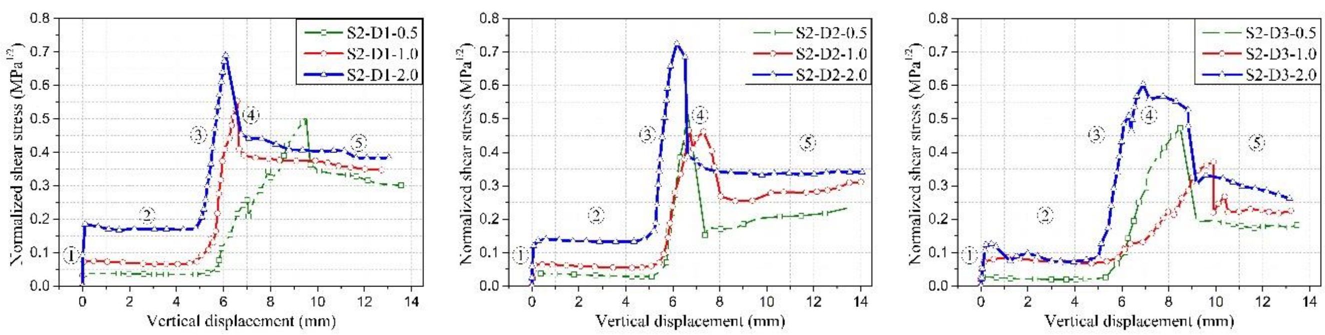

(a) (b) (c)

Fig. 9 Normalized shear stress–vertical displacement relations for gap joint specimens

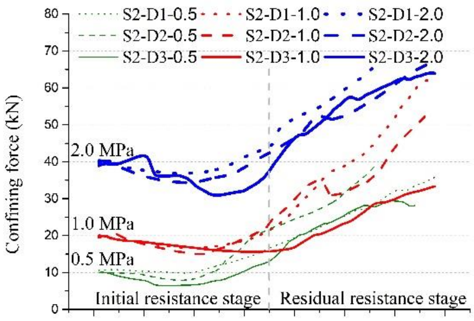

Fig. 10 Confining force recordation when testing gap joint specimens

protuberances rubbed down as the displacement progressed. Reduction of confining force at initial resistance stage was significant as well, as illustrated in Fig. 10.

The third stage: As test developed, the male key bottom contacted the female concave surface. The shear resistance comprised the contribution of friction resistance and support capacity of shear key. The ascending curve represented the applied load to overcome the overall shear resistance. The shear key progressively cracked in the shear plane, weakening the support capacity itself. At the end of this stage, ultimate shear capacity was reached.

The fourth stage: Up to a point when the failure of shear key base took place, the applied load dropped suddenly and the fracture ran through the entire joint. Material damage was also evident, thus large deformation took place. Especially, only the data of ultimate load and the data after sudden dropping of the curve were recorded during the experiments, owing to the limitation of data acquisition ability.

The final stage (Residual resistance stage): After shear key was completely destroyed, the support capacity of shear key disappeared and only the friction coefficient activated, providing residual shear resistance. A failure plane appeared along shear key base, resulting in a very rough interface with aggregate exposed. Shear resistance then was sustained mainly via aggregate interlock of the rough surface and the friction of the smooth surface. Consequently, shear force at residual resistance stage is larger than that of initial resistance stage.

Problematic specimen: The curve of specimen S2-D3-1.0 was different from others, presenting that the displacement was larger and ultimate shear strength was reduced. As can be observed in Fig. 7(h), the failure pattern of specimen S2-D3-1.0 showed that concrete of the female part was severely crushed prior to ultimate shear failure, which reduced the stiffness and shear resistance. This crushing failure appeared, for the reason that the male key bottom contacted in the right bottom corner first, resulting in a severe compressive force acted on the female part. Apart from this specimen, the load-slip relations of other tests were quite similar.

4.3 Friction coefficient

Friction coefficient is calculated by friction force (the applied load) divided by normal force (horizontal confining force). The first fifteen values of friction coefficient at initial resistance stage and fifteen values after shear-off failure at residual resistance stage are presented in Fig. 11. Representative mean values for friction coefficient recommended by *fib* Model Code 2010 range 0.5-0.7, 0.7-1.0, and 1.0-1.4, corresponding to Smooth interface, Rough interface and Very rough interface, respectively.

Table 3 Results of friction coefficient at initial resistance stage

References	Specimen name	Friction coefficient	Concrete type
In this test	S2-D1-0.5	0.594	C65(HSC)
	S2-D1-1.0	0.645	C65(HSC)
	S2-D1-2.0	0.750	C65(HSC)
	S2-D2-0.5	0.594	C65(HSC)
	S2-D2-1.0	0.576	C65(HSC)
	S2-D2-2.0	0.620	C65(HSC)
	S2-D3-0.5	0.479	C65(HSC)
	S2-D3-1.0	0.715	C65(HSC)
	S2-D3-2.0	0.463	C65(HSC)
	Mean	0.604	
Jiang *et al.* (2015)	F-01	0.619	C40(NC)
	F-02	0.585	C40(NC)
	Mean	0.602	
Voo *et al.* (2015)	SK5-10	0.47	C148(UHPC)
	SK5-20	0.36	C148(UHPC)
	SK3-10	0.46	C148(UHPC)
	SK3-20	0.36	C148(UHPC)
	SK1-10	0.45	C149(UHPC)
	SK1-20	0.35	C149(UHPC)
	Mean	0.408	
AASHTO (2003)	--	0.6	--
ACI 318-14	Not intentionally roughened	0.6	--
	Intentionally roughened	1.0	--
fib Model Code 2010	Smooth interface	0.5 - 0.7	<=C50/60
	Rough interface	0.7 - 1.0	<=C50/60
	Very rough interface	1.0 - 1.4	<=C50/60

Note: -- Not explicitly defined. (HSC=high strength concrete, NC=normal concrete, UHPC=ultra-high performance concrete)

4.3.1 Initial resistance stage

In most cases, the values of friction coefficient at initial resistance stage were approximately in the ranges 0.5 - 0.7. Even though the polishing effect developed at initial resistance stage, friction coefficient did not change much, sustaining in a smooth interface level.

Mean values of friction coefficient at initial resistance stage are listed in Table 3. Mean value of all gap joint specimens was 0.604, irrespective of shear key depth and confining stress. Values of friction coefficient referring to papers (Jiang *et al.* 2015, Voo *et al.* 2015) and Codes (AASHTO 2003, ACI 318-14, *fib* Model Code 2010) are also listed in Table 3, considering the effect of concrete type, and the roughness of interface. The value of friction coefficient of normal concrete was 0.602, whereas those

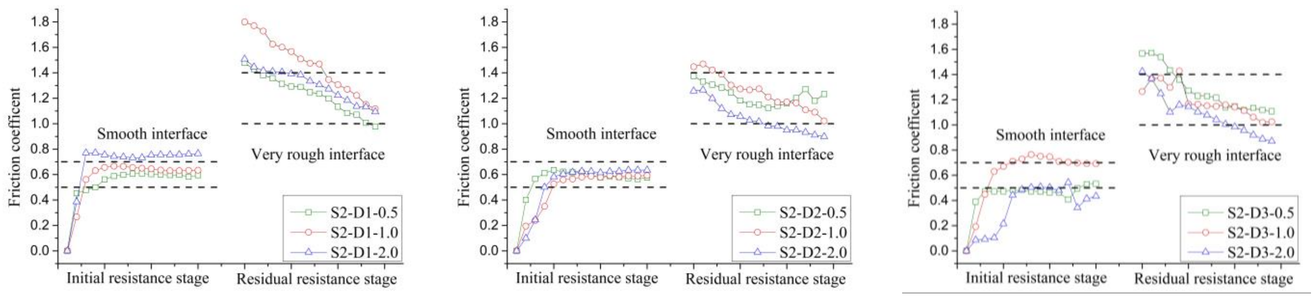

(a) (b) (c)

Fig. 11 Friction coefficient of gap joint specimens

Table 4 Results of support capacity of shear key

References	Specimens	Initial friction resistance (kN)	Shear capacity (kN)	Support capacity of shear key (kN)	Concrete type	Key number
In this test	S2-D1-0.5	6.03	84.39	78.36	C65(HSC)	Single key
	S2-D2-0.5	5.68	86.72	81.04	C65(HSC)	Single key
	S2-D3-0.5	3.85	78.50	74.65	C65(HSC)	Single key
	S2-D1-1.0	11.74	91.82	80.08	C65(HSC)	Single key
	S2-D2-1.0	9.60	77.60	68.00	C65(HSC)	Single key
	S2-D3-1.0	***12.71***	***61.64***	***48.93***	C65(HSC)	Single key
	S2-D1-2.0	28.76	114.62	85.86	C65(HSC)	Single key
	S2-D2-2.0	21.23	120.44	99.21	C65(HSC)	Single key
	S2-D3-2.0	16.31	100.31	84.00	C65(HSC)	Single key
Jiang *et al*. (2016b)	K1-S4-P-0.5	0	100.9	100.9	C40(SFRC)	Single key
	K1-S4-P-1.0	0	121.1	121.1	C40(SFRC)	Single key
	K1-S4-P-2.0	0	153.8	153.8	C40(SFRC)	Single key
Turmo *et al*. (2006)	PC-C	0	1077	1077	C40(PC)	Seven keys
	SFRC-C	0	945	945	C40(SFRC)	Seven keys

Note: Support capacity of shear key = Shear capacity - Initial friction resistance,
Initial friction resistance is defined as mean value of friction at initial resistance stage,
S2-D3-1.0 is problematic specimen. (SFRC=steel fiber reinforced concrete, PC=reinforced concrete)

values were 0.604 and 0.408 corresponding to high strength concrete and ultra-high performance concrete. It is reasonably believed that concrete type also had a contribution to friction coefficient of the flat part of single-keyed dry joint.

4.3.2 Residual resistance stage

Friction coefficient at residual resistance stage was much higher than that at initial resistance stage, approximately equal to representative mean values for a very rough interface, as presented in Fig. 11. Fracture of coarse aggregate changed the roughness of the interface. Friction coefficient at residual resistance stage presented an obvious decrease because of interface deterioration as an increasing slip.

Friction coefficient played an important role in shear strength at initial and residual resistance stage. As depicted in Fig. 9, shear strength at residual resistance stage was higher than that at initial resistance stage. As aforementioned, friction coefficient at residual resistance stage was higher than that at initial resistance stage. Confining force was another effective factor influenced shear strength. Confining force increased as vertical loading developed due to dilatation effect after the key bottom contacted in accordance with the results in Fig. 10. Therefore, it achieved higher shear strength at residual resistance stage.

4.4 Shear capacity and support capacity of shear key

Shear key plays an important role in mechanism for shear transfer, providing significant resistance and hindering the slippage. Shear capacity is the applied peak load obtained by the vertical load cell. Support capacity of shear key is calculated by shear capacity minus initial friction resistance.

Ultimate shear strength, which was defined as shear capacity divided by the area of the whole joint and $\sqrt{f_c^{'}}$, was plotted versus shear key depth of the gap joint specimen in Fig. 12. The effect of shear key depth showed the different results on the matching joint (Jiang *et al*. 2015) and the gap joint (the present test). There was a positive correlation between ultimate shear strength and shear key depth in matching joint specimens, whereas it showed a declined trend in gap joint specimens. The depth of 45 mm presented lowest values of ultimate shear strength than those of 25 mm and 35 mm in gap joint specimens, decreasing 6.98%, 32.87% (calculated by problematic

Table 5 Strength reduction and Code evaluation of gap joint specimens

Gap joint specimens	V_{E2}	Strength reduction			Code evaluation		
		Matching joint	V_{E1}	Reduced	V_A	V_{E1}/V_A	V_{E2}/V_A
S2-D1-0.5	84.39	S1-D2-0.5	105.43	19.96%	85.05	1.24	0.99
S2-D2-0.5	86.72	S1-D2-0.5	105.43	17.75%	85.05	1.24	1.02
S2-D3-0.5	78.50	S1-D2-0.5	105.43	25.54%	85.05	1.24	0.92
S2-D1-1.0	91.82	S1-D2-1.0	134.80	31.88%	95.70	1.41	0.96
S2-D2-1.0	77.60	S1-D2-1.0	134.80	42.43%	95.70	1.41	0.81
S2-D3-1.0	***61.64***	S1-D2-1.0	134.80	***54.27%***	95.70	1.41	***0.64***
S2-D1-2.0	114.62	S1-D2-2.0	164.30	30.24%	117.00	1.40	0.98
S2-D2-2.0	120.44	S1-D2-2.0	164.30	26.70%	117.00	1.40	1.03
S2-D3-2.0	100.31	S1-D2-2.0	164.30	38.95%	117.00	1.40	0.86
		Mean of reduced percentage: 31.97%, STDEV: 0.12			Mean of V_{E1}/V_A: 1.35, STDEV: 0.08 Mean of V_{E2}/V_A: 0.91, STDEV: 0.13		

Note: V_{E1}=Experimental shear capacity of the matching joint (kN), V_{E2}=Experimental shear capacity of the gap joint (kN), V_A=Shear capacity calculated by AASHTO (kN).

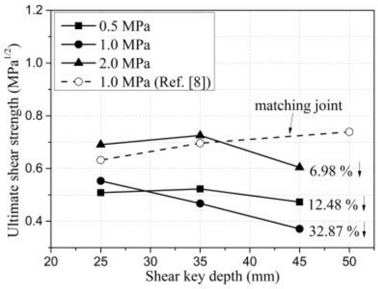

Fig. 12 Ultimate shear strength of the gap joint

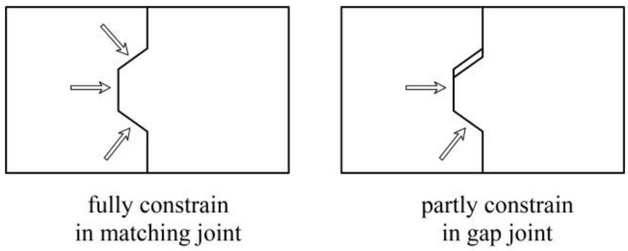

Fig. 13 Constrain acted on shear key

specimen) and 12.48% corresponding to specimens under 0.5 MPa, 1.0 MPa and 2.0 MPa confining stress. Confining stress could also influence ultimate shear strength. Compared with mean values of specimens under 0.5 and 1.0 MPa confining stress, applying 2.0 MPa confining stress enhanced shear capacity of the gap joint significantly. To obtain a higher shear capacity of the gap joint, deeper shear key should be avoided and higher confining stress should be provided.

Support capacity of a shear key had a significant contribution to shear capacity of keyed joint specimens. Table 4 summarizes the test results, including initial friction resistance, shear capacity and support capacity of shear keys. Under confining stress of 2.0 MPa, support capacity of shear key achieved the highest values than those of 0.5 MPa and 1.0 MPa. Confining stress made the shear key turned out to be small prestressed concrete corbel, increasing support capacity of shear key with compression. Table 4 also lists the data about support capacity of shear keys obtained from previous researches (Jiang *et al*. 2016b, Turmo *et al*. 2006), concerning about confining stress, concrete type and the number of shear keys. The results of Jiang *et al*. showed that support capacity of a shear key increased as confining stress increased. The results of Turmo *et al*. indicated that adding steel fiber in concrete did not increase support capacity of shear keys.

5. Strength reduction of shear capacity

Shear capacity of gap joint specimens were obviously lower than those of matching joint specimens. The reduced percentages of shear capacity between the gap joint and the matching joint were presented in Table 5. Strength reduction of gap joint specimens ranged from 17.75% to 42.43%, but the problematic specimen reduced 54.27%. Mean values of reduced percentage and standard deviation were 31.97% and 0.12, respectively. Such a significant strength reduction was caused by the weakening effect of partly constraint on shear key. As depicted in Fig. 13, shear key in the matching joint specimen was fully constraint, but shear key in the gap joint specimen was partly constraint. In addition, experimental gap joint specimens might partial contact at left or right bottom. Partial contact would significantly decrease shear capacity, which was confirmed in the following numerical simulation.

As recommended in AASHTO (2003) provision, shear capacity of the dry joint specimen is calculated by the following formula

$$V = A_k \sqrt{f_c'}\,(0.9961 + 0.2048\sigma_n) + 0.6A_{sm}\sigma_n \tag{1}$$

Where: areas of all shear keys base in the failure plane A_k (m^2), compressive strength of concrete f'_c (MPa), normal compressive stress in concrete after allowance for all prestress losses determined at the centroid of the cross section σ_n (MPa), and the area of contact between smooth surfaces on the joint A_{sm} (m^2).

Code evaluation was the ratio of experimental shear capacity to the calculated shear capacity using AASHTO provision and the results are presented in Table 5. As expected, AASHTO provision underestimated shear capacity of all matching joint specimens. Mean of the ratio of experimental shear capacity to the calculation by

AASHTO was 1.35, and standard deviation was 0.08. However, shear capacity of experimental results of most gap joint specimens were lower than those calculated values but approached the calculations. Mean of the ratio of experimental shear capacity to the AASHTO value was 0.91, and standard deviation was 0.13. Consequently, it was reasonable to draw a conclusion that AASHTO provision gave an accurate prediction for shear capacity of the gap dry joint in PCSBs.

Although match-casting-free construction method might significantly reduce shear capacity of PCSBs, it is possible to enhance shear capacity of the gap joint specimen, such as using high performance concrete and applying higher confining stress. The value of match-casting-free construction reflects in technological advance on construction speed and economic benefit. More researches should be carried out to study the applicability and improvement of the gap joint in PCSBs.

6. Numerical simulation

6.1 Problems to be solved

Contacting locations: Due to a gap in the joint, there are three cases of different results at where shear key bottom contacts the concave bottom surface, including full contact, right contact and left contact. In order to obtain an accurate result on shear behavior of the gap joint, these cases are analyzed in the following parametric study.

The gap height: Compared with traditionally matching joint specimens, the gap in shear key maybe influences shear force transfer of gap joint specimens. In this research, the gap height is totally 10 mm. It is reasonable to assume that narrowing the height of the gap may enhance shear capacity of gap joint specimens.

The height of shear key base: According to AASHTO formula, the area of shear key base is positive with shear capacity of keyed joint. The large increment in the height of shear key base is likely to be an effective way to enhance shear capacity of gap joint specimens.

6.2 Description of the model

In the numerical simulation, the parameters of the finite-element models include contacting locations of shear key bottom, the gap height and the height of shear key base. Both matching joint specimens and gap joint specimens are modeled in ABAQUS 6.14. The concrete damage plasticity (CDP) model is selected to simulate concrete cracking in the elastic-plastic behavior, which allows the inelastic behavior of concrete. The dilation angle, the eccentricity of flow and the viscosity coefficient are set as 36, 0.1 and 0.001, respectively. The ratio of biaxial strength to uniaxial strength is f_{bo}/f_{co}=1.16.

A three-dimensional solid model consists of two independent parts in contact, which keys and joints are modeled using the geometry of experimental specimens. A finer mesh is used for the shear key and a coarser mesh for the rest of the model. All the displacement of the bottom surface was restricted. Furthermore, a surface-to-surface contact interaction and the hard contact model are chosen. In this model, the material properties use the data obtained from the test day in Table 2.

6.3 Calibration of the model

To improve the validity of the numerical simulation, the finite element models are calibrated against the experimental results of matching joint specimens. The simulated results and experimental ones are compared on load-displacement curves (Fig. 14) and cracking failure patterns (Figs. 2, 5 and 15).

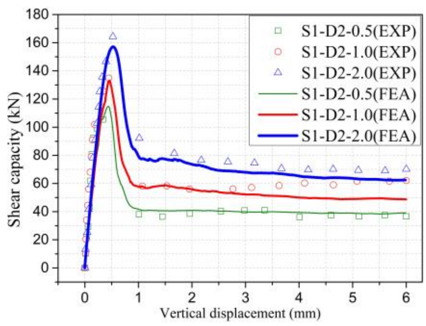

Fig. 14 Numerical and experimental load-displacement curves of the matching joint

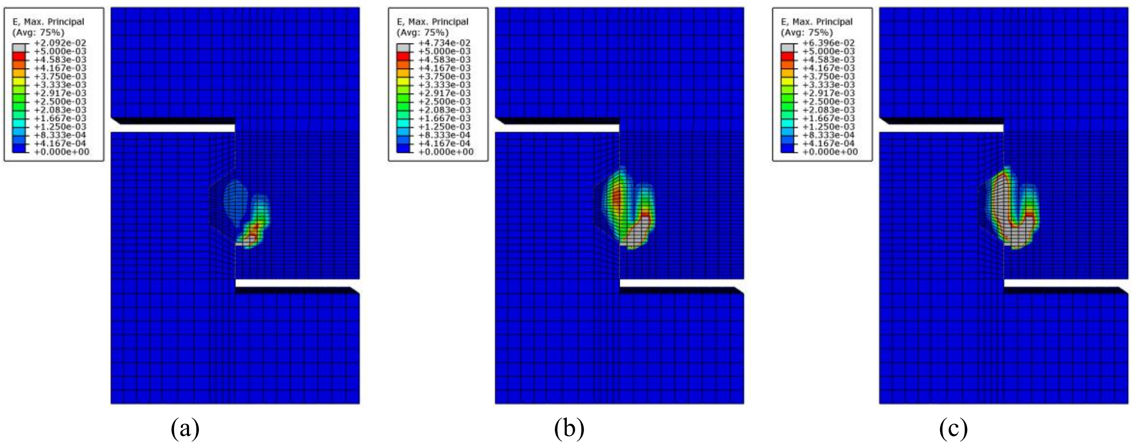

(a) (b) (c)

Fig. 15 Numerical failure crack propagating patterns of matching joint specimens

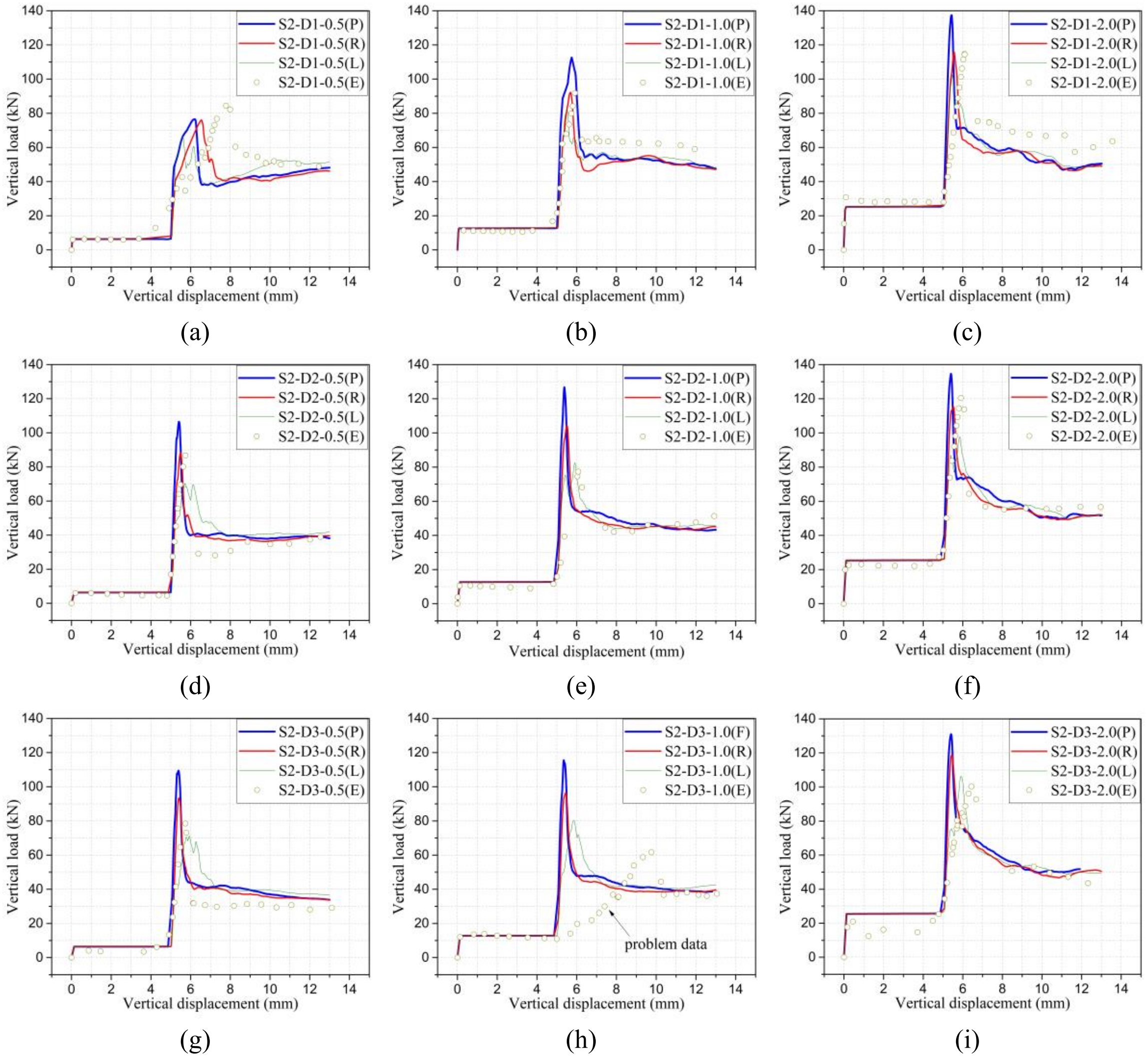

Fig. 16 Vertical load–vertical displacement relations (contacting locations) Full contact (F), Right contact (R), Left contact (L), and Experimental results (E)

As depicted in Fig. 14, the experimental results are presented as the scattered dots, while the finite element model analysis results are shown as the dashed or solid line. It can be found that the simulated curves and the test data points are approximately similar. The mean values and standard deviation of the ratio of numerical results to experimental ones are 1.01 and 0.07, respectively. This indicates that the numerical results are in good agreement with the test and give an acceptable prediction.

This simulated cracking failure propagation (Fig. 15) is consistent with those of the experimental results (Fig. 5) and typical failure mode (Fig. 2), with a single curvilinear crack beginning at shear key bottom corner and principle destroyed crack along with the vertical shear key base plane. In order to express the cracking, the area will be illustrated in gray where the tension strain has exceeded the ultimate tensile strain of concrete.

Consequently, it is acceptable to use the numerical method to investigate shear behavior of keyed dry joint specimens in PCSBs. Because of the indeterminacy of contacting location in gap joint specimens in the experimental test, with the finite element model, this deficiency can be eradicated and it can also comprehensively reveal phenomenon of shear behavior of gap joint specimens.

6.4 Results of parametric analysis

6.4.1 Effect of contacting locations

One of the problems remained to be solved as aforementioned was that various contacting locations would lead to different results. The following cases were analyzed: full contact (male key bottom parallelled to female concave bottom), right contact (shear key base was 0.5 mm larger than that of full contact) and left contact (shear key base was 0.5 mm smaller than that of full contact). Numerical and experimental load-displacement curves were plotted in Fig. 16.

As presented in Table 6, contact locations made a great influence in shear capacity of gap joint specimens. The ratio of numerical results to AASHTO calculations ranged from 1.12–1.32 (one is 0.90), 0.89–1.10 and 0.72–1.07, corresponding to full contact, right contact and left contact respectively. For all of numerical results, full contact

Table 6 Numerical results of gap joint specimens

Specimens	Numerical results: Contacting location	Numerical results: V_N (kN)	Code evaluation: V_A (kN)	Code evaluation: V_N/V_A	Experimental results: V_{E2} (kN)	Experimental results: V_N/V_{E2}
S2-D1-0.5	Full	76.47	85.05	0.90	84.39	0.91
	Right	75.99	85.05	0.89	84.39	0.90
	Left	66.18	85.05	0.78	84.39	0.78
	Mean	72.88	85.05	0.86	84.39	0.86
S2-D1-1.0	Full	112.63	95.70	1.18	91.82	1.23
	Right	92.19	95.70	0.96	91.82	1.00
	Left	82.09	95.70	0.86	91.82	0.89
	Mean	95.64	95.70	1.00	91.82	1.04
S2-D1-2.0	Full	137.33	117.00	1.17	114.62	1.20
	Right	115.80	117.00	0.99	114.62	1.01
	Left	102.21	117.00	0.87	114.62	0.89
	Mean	118.45	117.00	1.01	114.62	1.03
S2-D2-0.5	Full	106.49	85.05	1.25	86.72	1.23
	Right	88.10	85.05	1.04	86.72	1.02
	Left	69.73	85.05	0.82	86.72	0.80
	Mean	88.11	85.05	1.04	86.72	1.02
S2-D2-1.0	Full	126.71	95.70	1.32	77.32	1.64
	Right	104.41	95.70	1.09	77.32	1.35
	Left	82.54	95.70	0.86	77.32	1.07
	Mean	104.55	95.70	1.09	77.32	1.35
S2-D2-2.0	Full	134.60	117.00	1.15	120.44	1.12
	Right	115.49	117.00	0.99	120.44	0.96
	Left	86.91	117.00	0.74	120.44	0.72
	Mean	112.33	117.00	0.96	120.44	0.93
S2-D3-0.5	Full	109.39	85.05	1.29	78.50	1.39
	Right	93.37	85.05	1.10	78.50	1.19
	Left	70.62	85.05	0.83	78.50	0.90
	Mean	91.13	85.05	1.07	78.50	1.16
S2-D3-1.0	Full	115.48	95.70	1.21	***61.64***	1.87
	Right	96.32	95.70	1.01	***61.64***	1.56
	Left	80.09	95.70	0.84	***61.64***	1.30
	Mean	97.30	95.70	1.02	***61.64***	1.58
S2-D3-2.0	Full	130.98	117.00	1.12	100.31	1.31
	Right	118.51	117.00	1.01	100.31	1.18
	Left	106.32	117.00	0.91	100.31	1.06
	Mean	118.60	117.00	1.01	100.31	1.18

Note: V_N = Numerical shear capacity, V_A = Shear capacity calculated by AASHTO, V_{E2} = Experimental shear capacity of the gap joint.

Table 7 Effect of the gap height on numerical shear capacity (Full contact)

Joint type	The gap height (mm)	V_N (kN)	Increasing percentage	V_A (kN)
Gap joint	5 mm	106.49	0.00%	85.05
	4 mm	107.09	0.56%	86.88
	3 mm	108.18	1.02%	88.70
	2 mm	111.39	2.97%	90.52
	1 mm	111.58	0.17%	92.34
Matching joint	0 mm	114.80	2.89%	94.17

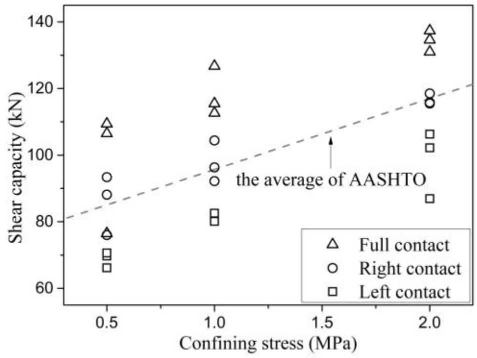

Fig. 17 Code evaluation of numerical results

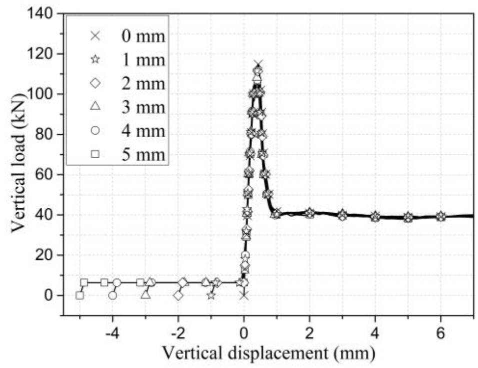

Fig. 18 Numerical load–displacement relations

specimens would get the highest shear capacity than other cases, because partial contact would result in local failure under stress concentration. The integrity of shear key was destroyed, thus shear capacity significantly decreased in case of partial contact both at left and at right. The case of left contact got the lowest shear capacity because the support capacity of shear key was significantly weakened.

Code evaluation was depicted in Fig. 17. The average line was plotted by AASHTO formula. It was obvious that shear capacity of full contact specimens was greater than the average, indicating that AASHTO provision underestimated them, namely, their shear resistance can be guaranteed. Right contact specimens showed a relative better agreement with AASHTO provision. Nevertheless, shear capacity of left contact specimens was obviously below the average, showing that AASHTO provision overe stimated them. Therefore, it was not suitable to predict shear capacity of gap joint specimens of left contact by the existing AASHTO formula. Hence, some strength reduction factors should be introduced to AASHTO formula.

6.4.2 Effect of the gap height

It is reasonable to assume that narrowing the gap's height (corresponding to change shear key base in height) would change shear capacity of gap joint specimens. The values of the gap height ranged from 1 to 5 mm in the numerical simulation, while shear key depth was 35 mm and under initial confining stress of 0.5 MPa. The numerical value of the matching joint (namely 0 mm gap in shear key) was also obtained. Load-displacement relationships were plotted in Fig. 18. In case of avoiding local failure due to partial contact, male key bottom was parallel to female concave bottom. As shown in Table 7, narrowing the gap

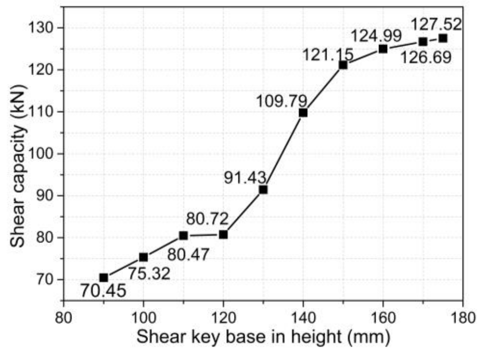

Fig. 19 Effect of shear key base on numerical shear capacity (Left contact)

height would increase shear capacity of gap joint specimens. Increasing percentages of shear capacity were 0.17%-2.89% when reducing per gap height. Therefore, it was not an effective and significant way to enhance shear capacity of gap joint specimens by means of narrowing the gap height.

6.4.3 Effect of the height of shear key base

It may be an effective way to increase shear capacity of gap joint specimens by increasing the height of shear key base. Shear key base area has a positive effect on shear capacity of gap dry joints according to AASHTO formula. For this purpose, gap joint specimens S2-D2-0.5 were modeled with shear key base of 90 to 175 mm in height of left contact, while shear key joint thickness kept constant. As depicted in Fig. 19, shear capacity was significantly improved since a larger shear key base strengthened the support capacity. Shear capacity increment gradually slowed down after shear key base was over 150 mm in height. As the height of shear key base increased from 90 to 150 mm, shear capacity increased by more than 1.5 times. Hence, in order to enhance shear capacity, the larger shear key base was recommended as well.

As mentioned above, consequently, methods to improve shear capacity of gap joint specimens can be summarized as following. Shear key bottom of partial contact should be avoided, and full contact as much as possible was recommended. Furthermore, larger shear key base positively strengthened the support capacity of shear key itself.

7. Conclusions

This research carries out experimental test and numerical simulation to investigate shear behavior of single-keyed dry joints in PCSBs with match-casting and match-casting-free construction, i.e. matching joints and gap joints. Failure behavior and shear capacity of the matching joint and the gap joint were compared. Based on experimental results and numerical analysis, the conclusions can be drawn as follows:

Experimental study:

For gap joint specimens, friction coefficient at residual resistance stage was much higher than that at initial resistance stage, since coarse aggregate exposed in the cracked interface. Friction coefficient at residual resistance stage presented an obvious decrease since increasing slip caused the interface deterioration.

The depth of 45 mm presented the lowest values of ultimate shear strength than those of 25 mm and 35 mm in gap joint specimens. Applying higher confining stress, at least 2.0 MPa, would improve shear capacity of the gap joint. Thus, deeper shear keys should be avoided and higher confining stress should be provided to achieve a higher shear capacity for a gap dry joint.

Compared with matching joint specimens, shear capacity of gap joint specimens was significantly decreased, ranged from 17.75% to 42.43%, mainly resulting from the weakening effect of partial constraint on shear key. AASHTO provision underestimated shear capacity of the matching joint specimens, but gave an accurate prediction for the gap joint specimens.

Numerical simulation:

Numerical simulation showed that shear capacity significantly decreased when partial contact both at left and at right. Code evaluation of full contact specimens proved that their shear capacity is greater than the average predicted by the AASHTO formula, while partial contact specimens' shear capacity is below the average. Therefore, the recommended method to improve shear capacity of gap joint specimens was full contact of shear key bottom.

This research also revealed that narrowing the gap height cannot remarkably enhance shear capacity of gap joint specimens. However, shear capacity was significantly improved by increasing the height of shear key base in the gap dry joint.

AASHTO provision underestimated shear capacity of full contact specimens, but overestimated that of left contact specimens, and gave a better prediction for right contact specimens. It is therefore suggested that some strength reduction factors should be introduced to AASHTO formula when applying it to a gap dry joint in PCSBs.

Acknowledgments

The research described in this paper was financially supported by National Natural Science Foundation of China [51778150, 51808133], Natural Science Foundation of Guangdong Province in China [2016A030313699], Science and Technology Planning Project of Guangzhou city in China [201804010422], and Special Founds for the Cultivation of Guangdong College Students' Scientific and Technological Innovation [pdjh2020b0179]. The authors gratefully acknowledge the helpful advice given by Prof. A.K.H. Kwan at The University of Hong Kong on the idea of "match-casting-free".

References

AASHTO (2003), Guide Specifications for Design and Construction of Segmental Concrete Bridges: 2003 interim

revisions, 2nd Edition, AASHTO, Washington, DC.
ACI (American Concrete Institute) (2014), Building Code Requirements for Structural Concrete, ACI 318-14, Farmington Hills, MI.
Alcalde, M., Cifuentes, H. and Medina, F. (2013), "Influence of the number of keys on shear strength of post-tensioned dry joints", *Mater. Constr.*, **63**(310), 297-307. https://doi.org/10.3989/mc.2013.07611.
Bu, Z. and Wu, W. (2018), "Inter shear transfer of unbonded prestressing precast segmental bridge column dry joints", *Eng. Struct.*, **154**(1), 52-65. https://doi.org/10.1016/j.engstruct.2017.10.048.
Fédération Internationale du Béton (*fib*) (2010), Model Code 2010-First Complete Draft, Vol. 1, Technical Report, Bulletin 55, Lausanne, Switzerland.
Hussein, H.H., Sargand, S.M., Rikabi, F.T. and Steinberg, E.P. (2017), "Laboratory evaluation of ultrahigh-performance concrete shear key for prestressed adjacent precast Concrete box girder bridges", *J. Bridge Eng.*, **22**(2), 04016113. https://doi.org/10.1061/(ASCE)BE.1943-5592.0000987.
Jang, H.O., Lee, H.S., Cho, K. and Kim, J. (2017), "Experimental study on shear performance of plain construction joints integrated with ultra-high performance concrete (UHPC)", *Constr. Build. Mater.*, **152**, 16-23. https://doi.org/10.1016/j.conbuildmat.2017.06.156.
Jiang, H., Chen, L., Ma, Z.J. and Feng, W. (2015), "Shear behavior of dry joints with castellated keys in precast concrete segmental bridges", *J. Bridge Eng.*, **20**(2), 04014062. https://doi.org/10.1061/(ASCE)BE.1943-5592.0000649.
Jiang, H., Chen, Y., Liu, A., Wang, T. and Fang, Z. (2016a), "Effect of high-strength concrete on shear behavior of dry joints in precast concrete segmental bridges", *Steel Compos. Struct.*, **22**(5), 1019-1038. https://doi.org/10.12989/scs.2016.22.5.1019.
Jiang, H., Feng, J., Liu, A., Liang, W., Tan, Y. and Liang, H. (2019), "Effect of specimen thickness and coarse aggregate size on shear strength of single-keyed dry joints in precast concrete segmental bridges", *Struct. Concrete*, **20**(3), 955-970. https://doi.org/10.1002/suco.201800054.
Jiang, H., Wei, R., Ma, Z.J., Li, Y. and Jing, Y. (2016b), "Shear strength of steel fiber-reinforced concrete dry joints in precast segmental bridges", *J. Bridge Eng.*, **21**(11), 04016085. https://doi.org/10.1061/(ASCE)BE.1943-5592.0000968.
Kaneko, Y., Connor, J.J., Triantafillou, T.C. and Leung, C.K. (1993), "Fracture mechanics approach for failure of concrete shear key. I: Theory", *J. Eng. Mech.*, **119**(4), 681-700. https://doi.org/10.1061/(ASCE)0733-9399(1993)119:4(681).
Kim, H.S., Chin, W.J., Cho, J.R., Kim, Y.J. and Yoon, H. (2015), "An experimental study on the behavior of shear keys according to the curing time of UHPC", *Eng.*, **7**, 212-218. http://dx.doi.org/10.4236/eng.2015.74017.
Lee, C.H., Chin, W.J., Choi, E.S. and Kim, Y.J. (2011), "An experimental study on the joints in ultra high performance precast concrete segmental bridges", *J. Korea Concrete Inst.*, **23**(2), 235-244. (in Korean) https://doi.org/10.4334/JKCI.2011.23.2.235.
Liu, T., Wang, Z., Guo, J. and Wang, J. (2019), "Shear strength of dry joints in precast UHPC segmental bridges: experimental and theoretical research", *J. Bridge Eng.*, **24**(1), 04018100. https://doi.org/10.1061/(ASCE)BE.1943-5592.0001323.
Shamass, R., Zhou, X. and Alfano, G. (2015), "Finite-element analysis of shear-off failure of keyed dry joints in precast concrete segmental bridges", *J. Bridge Eng.*, **20**(6), 04014084. https://doi.org/10.1061/(ASCE)BE.1943-5592.0000669.
Turmo, J., Ramos, G. and Aparicio, A.C. (2006), "Shear strength of dry joints of concrete panels with and without steel fibres-Application to precast segmental bridges", *Eng. Struct.*, **28**(1), 23-33. https://doi.org/10.1016/j.engstruct.2005.07.001.
Turmo, J., Ramos, G. and Aparicio, A.C. (2012), "Towards a model of dry shear keyed joints: modelling of panel tests", *Comput. Concrete*, **10**(5), 469-487. https://doi.org/10.12989/cac.2012.10.5.469.
Voo, Y., Foster, S. and Voo, C.C. (2015), "Ultrahigh-performance concrete segmental bridge technology: toward sustainable bridge construction", *J. Bridge Eng.*, B5014001. https://doi.org/10.1061/(ASCE)BE.1943-5592.0000704.
Wang, M., Zhang, Y.T. and Tian, W. (2014), "The key technology of short-line matching method in precast segment assembling of externally prestressed concrete bridges", *Adv. Mater. Res.*, **7**, 1065-1069. https://doi.org/10.4028/www.scientific.net/AMR.1065-1069.912.
Williams, C.S., Massey, J.B., Bayrak, O. and Jirsa, J.O. (2017), "Investigation of interface shear transfer using push-through tests", *ACI Struct. J.*, **114**(1), 173-185. https://doi.org/10.14359/51689162.
Zhou, X., Mickleborough, N. and Li, Z. (2005), "Shear strength of joints in precast concrete segmental bridges", *ACI Struct. J.*, **102**(1), 3-11.

CC